Journal of Forestry, 2023, **121**, 262–271
https://doi.org/10.1093/jofore/fvad008
Advance access publication 18 April 2023
Research Article - geospatial technologies

OXFORD

Improving Deciduous Forest Inventory Plot Center Measurement Using Unoccupied Aerial Systems Imagery

Joshua Carpenter,[1] Daniel Rentauskas,[1] Nikhil Makkar,[1] Jinha Jung,[1,*] and Songlin Fei[2]

[1]Lyles School of Civil Engineering, Purdue University, 550 Stadium Mall Drive, West Lafayette, IN 47907, USA.
[2]Forestry and Natural Resources, Purdue University, 715 W. State Street, West Lafayette, IN 47907, USA.

*Corresponding author's email: jinha@purdue.edu

Abstract

Field-based forest inventory plots are fundamental for many forest studies. These on-the-ground measurements of small samples of forested areas provide foresters with key information such as the size, abundance, health, and value of their forests. Recently, forest inventory plots have begun to be used as ground validation for tree features automatically extracted from remotely sensed data sets. Additionally, machine learning methods for feature extraction rely heavily on large quantities of training data and require these field forest inventory measurement datasets for algorithm training. Undermining the usefulness of forest inventory plot data as validation or training data is the positional uncertainty of plot location measurements. Because global navigation satellite systems (GNSS) cannot reliably measure plot center coordinates under thick tree canopy, plot center coordinates usually contain multiple meters of horizontal error. We present a method for reliably measuring plot center coordinates in which plot centers are individually marked with low-cost targets, allowing plot centers to be manually measured from orthoimagery captured during the leaf-off season. Our plot center measurements are shown to have less than 10 cm of horizontal error, an improvement of an order of magnitude over traditional GNSS methods.

Study Implications: Recently, as unoccupied aerial systems (UASs) make high-resolution data easy to collect, researchers have begun to develop methods for measuring individual tree features automatically from remotely sensed data. The output from these methods must be compared to on-the-ground measurements, most commonly to forest inventories. Although forest inventories provide accurate per tree characteristics, there is no method for measuring the global position of these inventories accurately and reliably. This prevents the ground measurements from matching up with remotely sensed datasets. This study introduces a method for using UASs to reliably measure the coordinates of plot centers to within 10 cm of true position.

Keywords: digital forestry, forest inventory, unmanned aerial system, unoccupied aerial vehicle, photogrammetry

Forests provide invaluable ecosystem services but are constantly challenged by climate change, disease outbreaks, and growing pressures from human population growth. Many forests across the globe have experienced an increase in tree mortality caused by the rising frequency and severity of fires, insects, disease, and extreme weather events (Allen, Breshears, and McDowell 2015; Fei et al. 2019; Hartmann et al. 2022). Some regions do not recover, whereas others experience shifts in the composition of tree species (Esquivel-Muelbert et al. 2019; Fei et al. 2017). As these changes become ubiquitous, the ability of ecosystems to continue to produce a diverse range of ecosystem services will become degraded and increasingly variable (Gauthier et al. 2014). In the face of these growing challenges, the forestry industry, the research community, and the public have begun to demand more data-driven decision-making and management founded on forest monitoring.

With the need for accurate wall-to-wall maps of forest biometric features never higher, research into the application of remote sensing technology for forest management and monitoring is garnering significant attention (Nitoslawski et al. 2021). Although forestry has been an early adopter of remote sensing technology, little progress has been made in tailoring the latest advances in automated feature extraction to the needs of foresters. Meanwhile, agriculture has taken advantage of the recent developments in remote sensing, paving the way for variable-rate fertilization, automated harvesting, and yield prediction (Ashapure et al. 2020). Research is now attempting to bring this digital revolution to the world of forestry (Choudhry and O'Kelly 2018; Nitoslawski et al. 2021).

Both imagery and Light Detection and Ranging (LiDAR) technologies have been leveraged to map features of the world's forests. Many forest features are detectable from satellite or airborne imagery. Tree density (Pinz 1991; Wulder, Niemann, and Goodenough 2000), canopy cover (Erker et al. 2019; Tang et al. 2019), and leaf area index (Dafeng Zhang et al. 2019) are all critical parameters that are extractable using spaceborne, airborne, or unoccupied aerial system (UAS) based imagery. One of the major benefits of remotely sensed data is the ability to measure relatively large forested areas at multiple time periods (Lechner, Foody, and Boyd 2020). This allows for benchmarking and subsequent monitoring of forest restoration efforts (Camarretta et al. 2020; Daowei Zhang 2019). The LiDAR technology is another remote sensing tool

Received: November 9, 2022. **Accepted:** February 24, 2023.

currently being used for forest inventory. This technology is renowned for its ability to capture height information; LiDAR data allows additional features to be detected from the air, such as trunk location (Zhao, Popescu, and Nelson 2009), canopy height (Oh et al. 2022), trunk diameter at breast height (DBH) (Feng et al. 2022), and crown shape (White et al. 2016) to mention a few.

The forest feature maps created by remote sensing data require validation. For high-resolution maps aiming to depict features at the scale of individual trees, the most reliable validation is on-the-ground measurement. This is where traditional forest inventories have been used. Although the exact protocol for completing traditional forest inventories varies based on region and jurisdiction, the basic components remain consistent. Forest inventories are in situ measurements of critical features of select trees within small sample plots dispersed throughout an area of interest (Fankhauser, Strigul, and Gatziolis 2018). Typically, these plots are marked with a center stake, especially for plots designed for repeated measures, and a fixed or variable radius is used to determine which trees fall within the plot (USDA Forest Service 2016). Although the primary purpose of forest inventories is to sample a population to determine the health, growth, characteristics, and value of the forest stand, the recent focus on creating high-resolution forest feature maps from remotely sensed data has turned these inventories into valuable validation or training data for mapping algorithms (Kangas et al. 2018).

To allow ground measurements to be matched with remotely sensed features, geographic correspondence between the inventory site and the remotely sensed data must be accurate. As the resolution of the extracted features increases, so too do the requirements for accuracy. For instance, as highlighted by Edson and Wing (2012), attempts to remotely sense individual tree attributes require direct correspondence between the positions of remotely sensed trees and their ground references. To establish this correspondence, some studies have used traditional survey methods by traversing with total stations to establish plot center coordinates (Tomaštík et al. 2017; Wing 2008), but typically, correspondence is established by measuring the global coordinates of the plot center using global navigation satellite systems (GNSS) (Falkowski et al. 2008; Næsset et al. 2004).

The unfortunate fact is that the forest environment causes significant errors in coordinate measurements taken with either handheld navigation-grade devices or survey-grade GNSS receivers. Navigation-grade devices provide a low-accuracy solution, usually without differential processing, and are intended for navigation. Their error is often in the order of multiple meters (Wing 2008). Higher accuracy dual-frequency receivers, which usually support differential processing, have also been used under the forest canopy. However, the accuracy of the measurements collected is unpredictable, with multi-meter errors common (Edson and Wing 2012; Naesset 2001). The resulting plot center location errors prevent the plot as a whole, and any subsequent inventory measurements that might be based on the erroneous coordinate, from being correctly mapped to the global reference frame. The USDA Forest Service has recognized this problem and has launched studies to develop more accurate methods for using GNSS to measure the global coordinates of their forest inventory and analysis plot centers to a higher degree of positional accuracy (Andersen, Strunk, and McGaughey 2022).

Errors in GNSS positioning within forested conditions are primarily caused by tree stems causing multipath or blocking the signal entirely. Multipath occurs when a satellite signal reflects off an object near the receiver, such as a tree trunk, causing the signal to deviate from the assumed direct path before reaching the receiver, degrading accuracy (Pirsiavash et al. 2019). Although modern GNSS receivers use hardware design, stochastic mitigation methods, and discriminator design to detect and remove multipath-infected signals (Trimble 2020), often, too few signals remain unblocked by trees or uncensored by multipath filters for any position solution to be calculated, even one with high positional dilution of precision (PDOP) (Edson and Wing 2012). Some work has concluded that high accuracy can be achieved after long periods of observation and using differential processing (Naesset 2001), prompting current protocols to recommend observations of many hours but not less than 15 minutes (Andersen, Strunk, and McGaughey 2022). However, as tree stems grow more densely together, their effect on the signals nullifies the potential gains of either long observations or differential processing (Edson and Wing 2012). Thus, although submeter accuracy is possible under the canopy with survey-grade GNSS, it is far from a guarantee. For high-resolution remote sensing data, even single-meter positional accuracies are not high enough to validate the performance of tree-feature mapping methods.

Many papers proposing high-resolution feature-mapping algorithms list the error caused by horizontal misalignment between remotely sensed data and the forest inventory measurements as a probable or significant source of error in validating feature extraction methods (Næsset et al. 2004). Fraser and Congalton (2019) describe the GNSS positional error of the forest inventory plot centers as a considerable concern that affected the level of confidence users could have in the statistical validity of the thematic maps. Hernández-Stefanoni et al. (2018) point out that the accuracy of their derived aboveground biomass decreases as the accuracy of the coregistration of the LiDAR data and field plots is degraded. For lower-resolution feature mapping, increasing the size of the area inventoried by on-the-ground measurements decreases the effect of misalignment on features derived from remotely sensed data (Hernández-Stefanoni et al. 2018; Mayamanikandan et al. 2022). However, if features are to be detected at a higher resolution than the plot size, or the ground validation plot cannot be expanded (as is the case when inventory plots have historic data), coordinate error must be considered. To correct for the geolocation error between the plots and imagery, Dafeng Zhang et al. (2019) resorted to sending field crews to the plot sites, marking the location of each tree on a printed aerial map, and then using these notes to manually match the field measurements to the corresponding trees.

In this study, we introduce a method for determining inventory plot centers to centimeter-level accuracy that is faster and more reliable than GNSS measurement. In our method, cost-effective targets are deployed at every plot center, then UAS imagery is captured over the area of interest during leaf-off conditions. After processing the imagery and correctly georeferencing the data, plot center coordinates are manually extracted from the orthoimagery. These steps allow plot center coordinates to be measured with precision and accuracy not currently available using handheld navigation-grade GNSS units nor guaranteed using survey-grade receivers.

Materials and Methods

Study Site

The site of this study was Martell Forest, a 470 acre research forest in northern Indiana, USA (40.44105,–87.03353). The forest is predominantly comprised of temperate hardwood species such as oaks and hickories. A total of 112 plots scattered throughout the forest have been monitored and updated regularly for several decades. Figure 1 shows the locations of all the plots throughout the forest.

Procedure

There were 112 forest inventory plot locations in this experiment. A target was placed at the center of each plot. Because of the large number of plots, the price per target needed to be as low as possible. We constructed our targets from 9-inch-wide strips of white house wrap, a water-resistant durable paper used for home construction that is available at most hardware stores. The paper was purchased on a 36-inch-wide roll and cut into four equal lengths with a carpenter's saw. In the field, a knife was used to cut two 1.5-meter-long strips, then these strips were placed on the ground in an "X" formation over the center of the plot and staked down with 6-inch nails. Figure 2 shows one target deployed at a plot center. The orange stake in the center of the target is an iron pipe placed in the ground decades ago when the plot was first established. We cut a slit in the target paper to accommodate the center monument.

In dense deciduous forests, the ground is often obscured by the canopy. To see the targets at the plot centers, flights could only be conducted during the leaf-off season. We deployed our targets during the early weeks of March 2022 and flew over the site on March 16, 2022. March was chosen because the weather in Indiana has warmed to the degree that there is little threat of snowfall covering the targets but leaf flushing has not yet occurred. To capture the images necessary to build an orthoimage of the forest, we used a Matrice 300 platform mounted with a Zenmuse P1 RGB camera (DJI, Shenzhen, China). The flight parameters are listed in Table 1. The flight over the entire 470 acres of Martell Forest took 6 hours to complete and collected nearly eight thousand images. During the flight, we used the INCORS INWL base station maintained by the Indiana Department of Transportation and the Matrice's RTK (real-time kinematic) capabilities to directly georeference each image. In this process, each image is tagged with the location of the camera at the time of capture. These locations are used during the photogrammetric reconstruction to constrain the camera locations, thereby improving accuracy and removing the requirement for ground control points (GCPs).

Although GCPs are not required when using direct georeferencing, we established seven GCPs in the flight area to validate the photogrammetric reconstruction. Their position can be seen in figure 3. The GCPs were composed of permanent ground features and checkerboard targets. Where distinct permanent ground features were present, these were used as GCPs, as future flights could use the same ground control

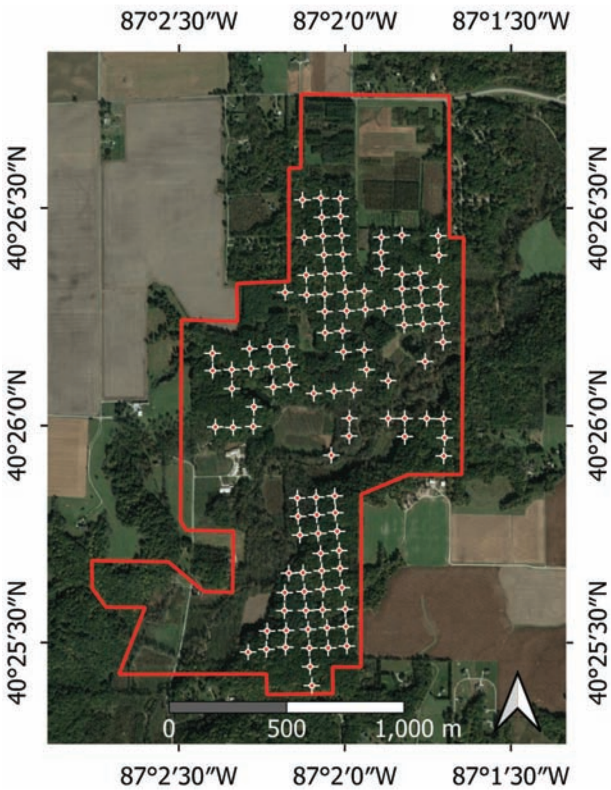

Figure 1. Map of Martell Forest, Indiana, USA. The outline shows the forest's boundaries. The crosses indicate the location of forest inventory plots.

Figure 2. A ground-based image of a forest inventory plot center and aerial target. The plot center is marked by a pipe.

Table 1. The flight parameters of the UAS photogrammetry mission

Altitude	120 m
Ground Sampling Distance	1.7 cm
Overlap	80%
Sidelap	80%

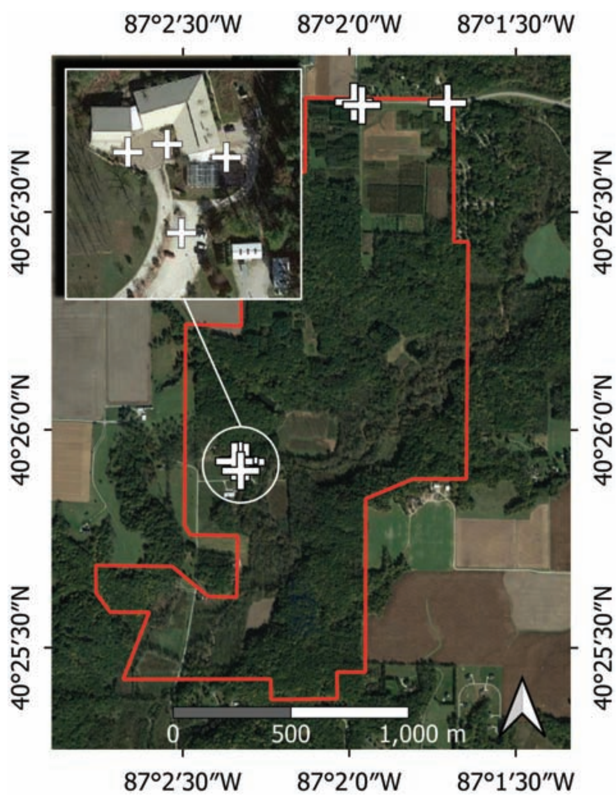

Figure 3. Map of Martell Forest, Indiana, USA. The crosses represent the position of permanent GCPs used to check the horizontal position of the orthoimage.

points. In areas where the ground was visible from the air but no permanent features could be found (e.g., large areas of open grassland), checkerboard targets were deployed. The positions of all GCPs were measured using the Reach RS2 (Emlid, Hong Kong, China) dual-frequency GNSS receiver using the INCORS INWL base station to perform RTK positioning.

After data collection, we processed the images to create a point cloud and orthoimage of the forest. The raw images were processed using the photogrammetric processing software Agisoft Metashape (version 1.7.1) (Agisoft, St. Petersburg, Russia). We followed the four-step procedure available in Metashape: align photos, build dense point cloud, build digital elevation model, and build orthomosaic. The "high accuracy" option was used to align photos. "Mild depth filtering" was implemented by Metashape while building the dense point cloud. Points that were reconstructed with only two images were manually filtered from the point cloud and then the digital surface model (DSM) and orthomosaic were created. The photogrammetric dense point cloud, the

Table 2. Absolute horizontal error of the 7 GCP coordinates determined after georeferencing by comparing target coordinates derived from the orthoimage to GNSS measurements.

Average error	0.016 m
Standard deviation	0.013 m
Maximum error	0.045 m

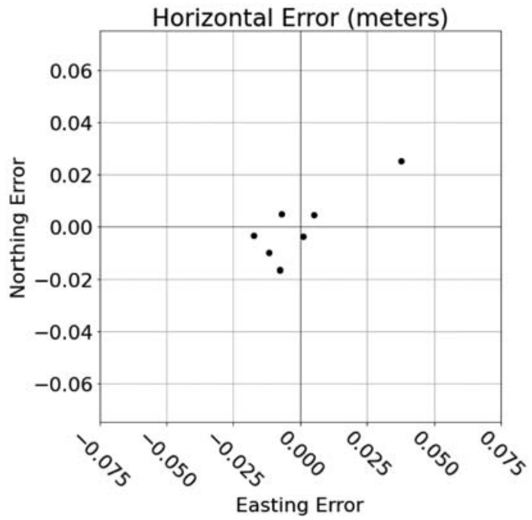

DSM, and the orthomosaic were exported from Metashape in the UTM Zone 16N (meters) projected coordinate system.

After reconstruction, the horizontal coordinates of the GCPs were sampled from the orthoimage using the Metashape interface. These were then compared with the coordinates measured during the GNSS survey. The difference between the two sets of horizontal coordinates was used to determine the linear shift to be applied to the data products, calculated by

$$T = \frac{\sum_{i=1}^{n} P_i - P'_i}{n}$$

where $T = \left[t_x \; t_y\right]^T$ is the shift moving the photogrammetric data products into the global reference frame, n is the number of GCPs ($n = 7$ in this experiment), P_i is the i-th GCP coordinate as extracted from the uncorrected orthoimage, and P'_i is the i-th GCP coordinate as measured by the GNSS survey. In our experiment, the shift T was computed to be

$$T = \left[0.010m \; - \; 0.018m\right]^T$$

After this shift was applied, the coordinates of the same GCPs used to calculate T were again sampled from the orthoimage and DSM. The absolute horizontal error between the sampled coordinates and the GNSS coordinates was then calculated; Table 2 shows the results. The average horizontal error was 1.6 cm, approximately equal to the ground sampling distance of the orthoimage (Table 1), with a standard deviation of 1.3 cm. This value describes the georeferencing precision of the orthoimage and photogrammetric point cloud.

Following the creation and correction of the photogrammetric data products, the next step was to digitize the plot centers from the orthoimage and point cloud. We used QGIS, an open-source software for viewing, editing, and creating geospatial databases, to view and digitize the orthoimage. The orthoimage was opened in this software and the coordinates were manually measured. Figure 4 shows a few examples of the plot center targets in the imagery. Although the coordinates were measured manually in this study to demonstrate the feasibility of this method, target extraction algorithms could be developed to automatically locate target centers if this location method were applied to a larger region.

For 5 of the 112 targets, the plot center target was too obscured by tree branches for an accurate coordinate to be measured from the orthoimage. Figure 5 shows one such case. Figure 5a shows the region of the orthoimage near a plot center target. The "swirling" patterns around the target are caused by noise in the photogrammetric point cloud that is propagated to the orthoimage. This happens most often where the thin branches of the upper canopy obscure the ground and provide few tie points for the image-matching routine built into Metashape's photogrammetric reconstruction process. In such areas, the horizontal position of objects in the orthoimage is unclear. For the five obscured targets, we opened the photogrammetric point cloud in CloudCompare to measure the plot center coordinates. Figure 5b shows the same plot center as viewed in the photogrammetric point cloud. The target position is evident in the point cloud, and its coordinates can be measured with a higher degree of certainty.

In general, it is preferred to measure plot center coordinates from the orthoimage. The orthoimage has two advantages over the photogrammetric point cloud. First, the orthoimage is easier to open and navigate because raster data generally requires less RAM than a high-resolution point cloud of the same area. The speed of opening and navigating raster data can also be improved by using the QGIS built-in pyramid building. Second, coordinate measurement on raster data is continuous. This allows the digitizer to measure the coordinate of the target centers without regard to pixel size or position. In point clouds, however, the digitizer is required to pick a specific point in the point cloud to represent the target center or, if no single point falls in the center of the target, must pick several points and interpolate a center. This adds further work and potential for error to the coordinate measurement procedure.

Figure 4. The inventory plot center targets as captured by the orthoimage. (a) Most targets were deployed in an X pattern. (b) However, based on ground conditions, forming an X shape was not always possible. In these cases, a half X was formed where the plot center can be located by finding the intersection of the legs of the half X.

Figure 5. In the orthoimage, occasionally the target may be obscured by branches (a). In these cases, the target can often be found more clearly in the photogrammetric point cloud (b).

Results

Accuracy Assessment

To evaluate the expected accuracy of the plot center coordinates derived using the method described above, the horizontal accuracy of the orthoimage georeferencing must be quantified along with the horizontal reliability of hand-digitized coordinates. The georeferencing accuracy of the orthoimage was calculated in the previous section and the results, shown in Table 2, indicate the georeferencing accuracy of the orthoimage to be 1.6 cm with a standard deviation of 1.3 cm. To determine the reliability of hand-digitized coordinates extracted from the orthoimage, we hand-digitized the coordinates of thirty permanent ground features scattered across the experiment site and compared them with coordinates digitized from a previous orthoimage of Martell created during the fall of 2021 using the same platform, flight parameters, and processing steps outlined above. Figure 6 shows the position of the permanent ground features used for this validation, and Figure 7 shows a few examples of these features.

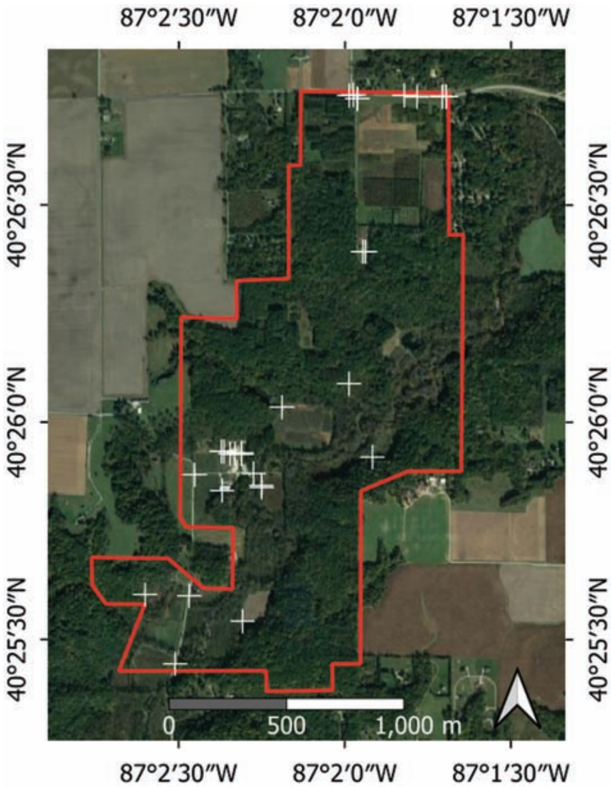

Figure 6. Map of Martell Forest, Indiana, USA. The crosses represent the position of permanent features used to check the reliability of manual coordinate measurement from the orthoimage.

The absolute error between a 2022 feature coordinate and its value as measured in 2021 was calculated as

$$\epsilon_i = \sqrt{\Delta x_i^2 + \Delta y_i^2}$$

where ϵ_i is the absolute horizontal error between test point i and validation point i, $\Delta x = x_i - x'_i$ is the change in the x coordinate between the i-th pair of 2022 and 2021 points, and $\Delta y = y_i - y'_i$ is the change in the y coordinate between the i-th pair of 2022 and 2021 points. The error found between all test and validation points is summarized in Table 3. We found the average horizontal error of hand-digitized points to be 2.3 cm with a standard deviation of 1.5 cm and a maximum error of 7.6 cm.

With both georeferencing accuracy and hand-digitization accuracy evaluated, the total positional uncertainty of the plot center measurements can be estimated. Given the following equations,

$$\epsilon_T = \epsilon_G + \epsilon_D$$

$$\sigma_T = \sqrt{\sigma_G^2 + \sigma_D^2}$$

where ϵ_T and σ_T are the expected error and standard deviation of the error in a plot center measurement, ϵ_G and σ_G are the expected error and standard deviation of the error georeferencing, and ϵ_D and σ_D are the expected error and standard deviation of the error in hand-digitization, we can calculate the estimated error in plot center coordinates measured using the proposed method to be

$$\varepsilon_T = 1.6 + 2.3 = 3.9cm$$

$$\sigma_T = \sqrt{1.3^2 + 1.5^2} = 2.0cm$$

indicating that any plot center coordinate measured with the proposed method likely contains about 4 cm of horizontal error with a standard deviation of 2 cm. It should be noted

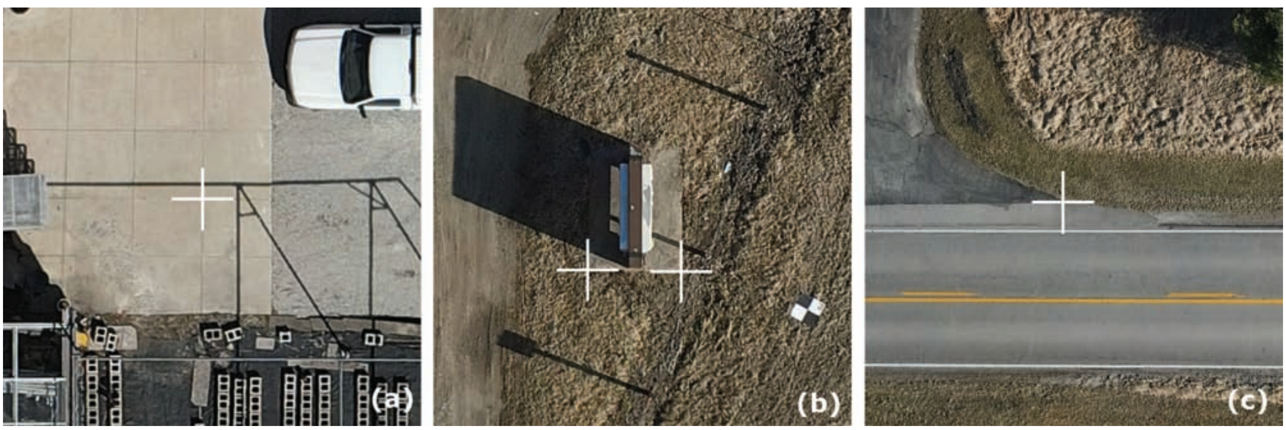

Figure 7. Examples of permanent objects used as comparison points. (a) The intersection of joint lines in a concrete patio. (b) The corners of a concrete sign pad. (c) The corner of an asphalt drive apron.

that this error is dependent on the ground sampling distance of the orthoimage. In this study, the average horizontal error is estimated at twice the ground sampling distance.

Plot Center Coordinate Improvement

To quantify the improvement achieved with our method, we calculate the absolute horizontal error between all 112 plot center coordinates extracted from the UAS imagery and the centers previously associated with each forest inventory. These previous coordinates had been measured with a navigation-grade GNSS receiver. These coordinates had been helpful for field crews looking for the plot centers, but, as our study shows, these coordinates did not have the necessary accuracy to correctly georeference the plot centers for comparison with high-resolution remotely sensed data. On average, the previous plot centers measured with navigation-grade receivers were 4.9 m different from our UAS-based measurements with a standard deviation of 4.3 m. These results are listed in Table 4. Figure 8 shows examples of the navigation-grade GNSS position along with the position extracted using the proposed method over the orthoimage.

Discussion

Experiment Design

A critique of the accuracy assessment (detailed in the Accuracy Assessment section) is that the hand-digitized coordinates of the plot centers were never compared with known values. Some other studies that have investigated plot center position have used total station traversing techniques to calculate high-accuracy plot center coordinates for validation (Edson and Wing 2012; Wing 2008; Tomaštík et al. 2017; Wing and Frank 2011). We decided against this method for three reasons. First, the size of the area for our experiments was significantly larger than in previous work. We implemented our method over 470 acres that contained 112 plot centers. Second, the time required to traverse through the forest to a statistically significant number of these plots was prohibitive. Finally, performing a complex traverse and achieving accurate and reliable results, especially in wooded and hilly conditions, is a difficult task even for experienced surveyors. Therefore, conducting a survey and using such data as validation would likely introduce more uncertainty into the accuracy of our work.

In this work, in lieu of a total station survey, we quantified the expected error in the georeferencing of the orthomosaic and then quantified the expected error introduced by hand-digitization. These two measures are then combined to determine the expected error for any features digitized from the georeferenced orthomosaic. As discussed in the Procedures section, if a local distortion in the orthomosaic was visually detected, the photogrammetric point cloud was used for digitizing the target. However, it must be acknowledged that there is some potential for minor positional errors in the photogrammetric reconstruction as branches move around during data collection, changing the patterns in the raw images used by Metashape to detect conjugate tie points. Although there is potential, the probability for this error is small because extensive point filtering was used during processing to avoid tie points found in a few images (the most likely tie points to be erroneous). Past research studying the accuracy of hand-digitized coordinates extracted from photogrammetric reconstructions of targets positioned under leaf-off canopy has found positional uncertainty similar to that presented in our work (Tomaštík et al. 2017).

It should also be noted that this study focused on the horizontal position of the plot centers for three reasons. First, aerial imagery is the most common remotely sensed data used in the forest environment. Features detected from imagery or other raster datasets often do not contain elevation data. Features are either planimetric or heights are relative, both of which do not need vertical information to accurately

Table 3. Absolute horizontal error between the coordinates of ground features hand-digitized from two different orthoimages of Martell Forest.

Average error	0.023 m
Standard deviation	0.015 m
Maximum error	0.076 m

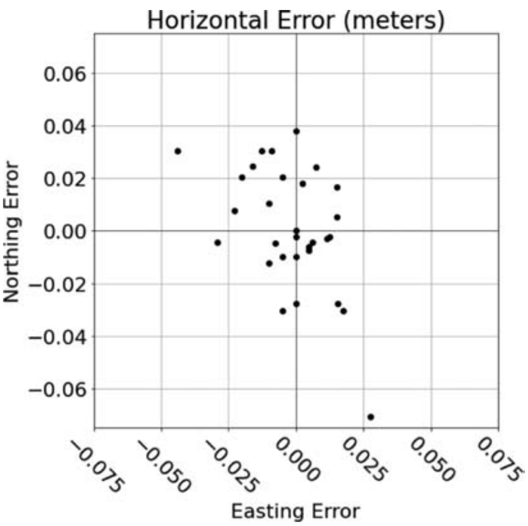

Table 4. Absolute horizontal error between GNSS-measured plot center coordinates and hand-digitized plot center coordinates.

Average error	4.875m
Standard deviation	4.372 m
Maximum error	28.225 m

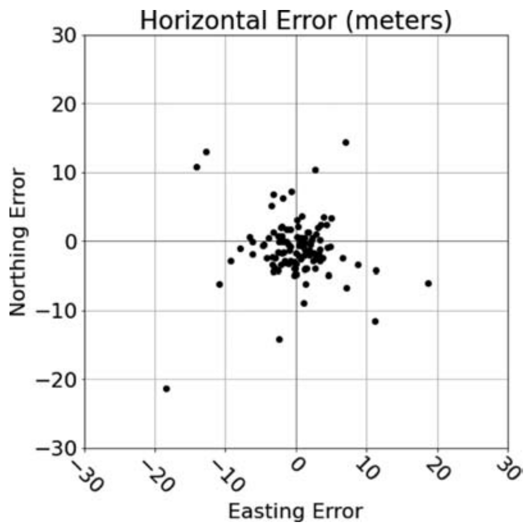

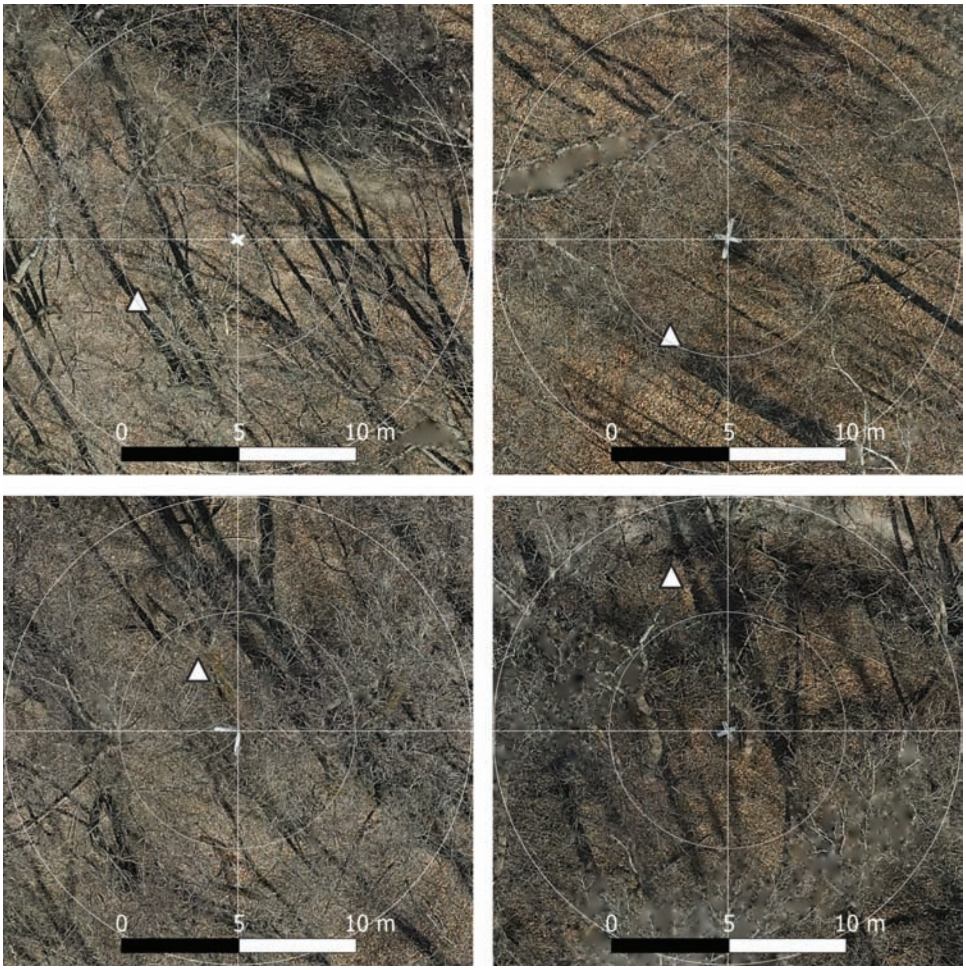

Figure 8. Comparison between the digitized plot centers and the GNSS measured centers of four select plots. The center of each tile indicates the position of the plot center target as digitized from the orthoimage. The GNSS center coordinates are marked by a triangle. Concentric circles are drawn at 5 m and 10 m radii from the plot center for scale reference. These four plots graphically show the improvement in plot center accuracy achieved by the digitization process presented in this article.

georeference plot centers for validation. Second, manual forest inventories usually do not encode vertical information. In manual forest inventories, typically an azimuth and distance to each tree within the plot are measured (USDA Forest Service 2016) and can be reduced to a local horizontal position for each tree; however, the vertical position of each tree is not measured. Therefore, improving the vertical position of the plot center does not add additional validation accuracy to individual tree positions.

Practical Considerations

Measuring the coordinates of plot centers from precisely georeferenced UAS-based orthoimagery provides highly accurate and precise results. However, not all plot centers require this level of precision. To determine whether a given task requires submeter plot center measurement, we suggest that the expected plot center coordinate error be compared against the resolution of the remotely sensed feature. If the expected coordinate error is significantly smaller than the output resolution of the extracted feature, improving the coordinate measurement accuracy is likely inconsequential. Our method is ideal for high-resolution applications where the desired features are smaller than the forest inventory plot size. At this level of desired output detail, where individual stems must be distinguished or individual canopies segregated, multiple meters of plot location error becomes significant. Studies that use the azimuth and distance from the plot center to each tree within the plot to locate individual trees for remotely sensed feature validation (Falkowski et al. 2008), are primary targets for this method. Næsset et al. (2004) point out that errors of only a few meters will introduce large variability in attempts to use field sample plots as training data to develop methods for completing forest-wide inventories.

An additional consideration when comparing the proposed methodology to other plot center coordinate measuring options is the use of UASs. The UASs are excellent tools for collecting high-resolution data over moderately sized areas. However, battery life and regulations that require line-of-sight contact between the vehicle and the pilot limit the acreage that can be covered easily. For very large continuous expanses of woodland, access and clearings for takeoff and landing may make flights difficult or impossible to execute. It is also critical to consider airspace restrictions when planning flights. In most jurisdictions, special permitting is needed to access restricted airspace, especially around airports. We anticipate the proposed method being used on midsized projects that require high-accuracy plot center coordinates, such as building validation datasets for further development of UAS-based forest inventory technology.

Although the method of creating an orthomosaic image and hand-digitizing features is a reliable method for measuring the coordinates of ground features, measuring features under the canopy requires line-of-sight from the UAS to the feature of interest. In nondeciduous forests, such as tropical forests or evergreen forests, meeting this requirement may be impossible. Our method is designed for deciduous forests or plot centers that are perennially visible from the sky.

Further, as implemented in this study, this method requires two visits to the plot location: a preflight visit to deploy the targets and a postflight visit to retrieve the targets. This takes time and effort. However, we determined that the time investment was less than that needed to complete long GNSS surveys and that the accuracy was superior to that available through GNSS. To remove the need for a second visit, we recommend using biodegradable products to construct the aerial targets. The house wrap used in this experiment can be substituted with tear-resistant biodegradable paper and wooden dowels can be used to pin the targets to the ground.

Contribution

Improved accuracy is the major advantage of our approach. This increase in accuracy is necessary for any high-resolution tree mapping methods that use forest inventory plots or any other ground-based sampling for validation. Our method ensures that these plot measurements are correctly georeferenced and align with remotely sensed data. It is best when used by projects that require UAS imagery. The orthoimagery and DSM created to locate plot center locations have the potential to be used for other purposes such as tree counts or terrain modeling.

In addition to improved accuracy of sample locations, our method can save time in the field. If accurate plot centers are required for a study, using survey-grade GNSS receivers can require hours of observation time for each point measured. Even after long observation times, the accuracy of the final coordinate is not guaranteed. In our experiment, two of the authors hiked to 112 plot centers, searched for, and found the ground monument, and placed the "X" target at an average rate of 15–20 minutes per plot. Because the targets are quick to deploy, the time per target represents only the time to hike and find each plot center—time that would be spent regardless of the survey method. By removing long observation times, we significantly reduce time spent in the field.

Not only does our method save time in the field, but it also improves the safety and efficiency of field crews. Traditional surveying tools such as total stations or survey-grade GNSS units are expensive, can be heavy, and require trained technicians to operate. In the forested environment, there are often hills and steep grades. These environments are often made more hazardous by the thick layers of fallen leaves and branches that accumulate on the forest floor. When hiking between plots located on uneven terrain, slips and trips are common. Carrying a survey-grade GNSS receiver mounted to the ubiquitous 2-meter-tall rod with a bipod or tripod increases the risk of equipment damage or personal injury. Our method removes the need for heavy, expensive equipment. Target material can be carried in a backpack, which makes hiking far more manageable and less risky. Additionally, far less experience is needed for field crews to deploy targets.

Conclusion

Having accurate forest inventory plot center coordinate measurement is a critical first step when using forest inventory plot data or other ground samples to validate the results of high-resolution forest features extracted from remote sensing data. Current methods of measuring plot centers often rely on navigation-grade or survey-grade GNSS receivers. However, both systems include significant horizontal uncertainty when measuring the coordinates of a point under the forest canopy. These positional errors degrade the validity of comparisons between field-based inventory data and remotely sensed features. We proposed a methodology for locating plot centers in deciduous forests to an accuracy of ±4cm. Compared with current plot coordinate measurement methods, this accuracy is an improvement of several orders of magnitude. This method requires targets to be deployed at the plot centers and UAS-based imagery to be collected during leaf-off conditions. Leaf-on conditions or dense conifer forests will obscure targets. The coordinates of the plots can then be manually measured from the resulting orthoimage.

This method significantly improves the accuracy and reliability of plot center coordinate measurements. It has the added benefit of saving time in the field, increasing safety, and being easily implemented by untrained personnel.

Funding

This research is partially supported by the Purdue Integrated Digital Forestry Initiative.

Conflict of Interest

No conflicts of interest to declare.

Literature Cited

Allen, C.D., D.D. Breshears, and N.G. McDowell. 2015. "On Underestimation of Global Vulnerability to Tree Mortality and Forest Die-off from Hotter Drought in the Anthropocene." *Ecosphere* 6 (8): art129. doi: 10.1890/ES15-00203.1.

Andersen, Hans-Erik, Jacob Strunk, and Robert J. McGaughey. 2022. "Using High-Performance Global Navigation Satellite System Technology to Improve Forest Inventory and Analysis Plot Coordinates in the Pacific Region." *Gen. Tech. Rep. PNW-GTR-1000*. Portland, OR: USDA Forest Service, Pacific Northwest Research Station.

Ashapure, A., J. Jung, A. Chang, S. Oh, J. Yeom, M. Maeda, A. Maeda, et al. 2020. "Developing a Machine Learning Based Cotton Yield Estimation Framework Using Multi-Temporal UAS Data." *ISPRS Journal of Photogrammetry and Remote Sensing* 169 (November): 180–194. doi: 10.1016/j.isprsjprs.2020.09.015.

Camarretta, N., P.A. Harrison, T. Bailey, B. Potts, A. Lucieer, N. Davidson, M. Hunt. 2020. "Monitoring Forest Structure to Guide Adaptive Management of Forest Restoration: A Review of Remote Sensing Approaches." *New Forests* 51 (4): 573–596. doi: 10.1007/s11056-019-09754-5.

Choudhry, H., and G. O'Kelly. 2018. "Precision Forestry: A Revolution in the Woods." *Paper, Forest Products & Packaging*. McKinsey & Company. https://www.mckinsey.com/industries/paper-forest-products-and-packaging/our-insights/precision-forestry-a-revolution-in-the-woods.

Edson, C., and M.G. Wing. 2012. "Tree Location Measurement Accuracy with a Mapping-Grade GPS Receiver under Forest Canopy." *Forest Science* 58 (6): 567–576. doi: 10.5849/forsci.11-015.

Erker, T., L. Wang, L. Lorentz, A. Stoltman, and P.A. Townsend. 2019. "A Statewide Urban Tree Canopy Mapping Method." *Remote*

Sensing of Environment 229 (August): 148–158. doi: 10.1016/j.rse.2019.03.037.

Esquivel-Muelbert, A., T.R. Baker, K.G. Dexter, S.L. Lewis, R.J.W. Brienen, T.R. Feldpausch, J. Lloyd, et al. 2019. "Compositional Response of Amazon Forests to Climate Change." *Global Change Biology* 25 (1): 39–56. doi: 10.1111/gcb.14413.

Falkowski, M.J., A.M. Smith, P.E. Gessler, A.T. Hudak, L.A. Vierling, and J.S. Evans. 2008. "The Influence of Conifer Forest Canopy Cover on the Accuracy of Two Individual Tree Measurement Algorithms Using Lidar Data." *Canadian Journal of Remote Sensing* 34 (sup2): S338–S350. doi: 10.5589/m08-055.

Fankhauser, K., N. Strigul, and D. Gatziolis. 2018. "Augmentation of Traditional Forest Inventory and Airborne Laser Scanning with Unmanned Aerial Systems and Photogrammetry for Forest Monitoring." *Remote Sensing* 10 (10): 1562. doi: 10.3390/rs10101562.

Fei, S., J.M. Desprez, K.M. Potter, I. Jo, J.A. Knott, and C.M. Oswalt. 2017. "Divergence of Species Responses to Climate Change." *Science Advances* 3 (5): e1603055. doi:10.1126/sciadv.1603055.

Fei, S., R.S. Morin, C.M. Oswalt, and A.M. Liebhold. 2019. "Biomass Losses Resulting from Insect and Disease Invasions in US Forests." *Proceedings of the National Academy of Sciences* 116 (35): 17371–17376. doi: 10.1073/pnas.1820601116.

Feng, B., S. Nie, C. Wang, X. Xi, J. Wang, G. Zhou, and H. Wang. 2022. "Exploring the Potential of UAV LiDAR Data for Trunk Point Extraction and Direct DBH Measurement." *Remote Sensing* 14 (12): 2753. doi: 10.3390/rs14122753.

Fraser, B.T., and R.G. Congalton. 2019. "Evaluating the Effectiveness of Unmanned Aerial Systems (UAS) for Collecting Thematic Map Accuracy Assessment Reference Data in New England Forests." *Forests* 10 (1): 24. doi: 10.3390/f10010024.

Gauthier, S., P. Bernier, P.J. Burton, J. Edwards, K. Isaac, N. Isabel, K. Jayen, et al. 2014. "Climate Change Vulnerability and Adaptation in the Managed Canadian Boreal Forest." *Environmental Reviews* 22 (3): 256–285. doi: 10.1139/er-2013-0064.

Hartmann, H., A. Bastos, A.J. Das, A. Esquivel-Muelbert, W.M. Hammond, J. Martínez-Vilalta, N.G. McDowell, et al. 2022. "Climate Change Risks to Global Forest Health: Emergence of Unexpected Events of Elevated Tree Mortality Worldwide." *Annual Review of Plant Biology* 73 (1): 673–702. doi: 10.1146/annurev-arplant-102820-012804.

Hernández-Stefanoni, J., G. Reyes-Palomeque, M. Castillo-Santiago, S. George-Chacón, A. Huechacona-Ruiz, F. Tun-Dzul, D. Rondon-Rivera, et al. 2018. "Effects of Sample Plot Size and GPS Location Errors on Aboveground Biomass Estimates from LiDAR in Tropical Dry Forests." *Remote Sensing* 10 (10): 1586. doi: 10.3390/rs10101586.

Kangas, A., R. Astrup, J. Breidenbach, J. Fridman, T. Gobakken, K.T. Korhonen, M. Maltamo, et al. 2018. "Remote Sensing and Forest Inventories in Nordic Countries – Roadmap for the Future." *Scandinavian Journal of Forest Research* 33 (4): 397–412. doi: 10.1080/02827581.2017.1416666.

Lechner, A.M., G.M. Foody, and D.S. Boyd. 2020. "Applications in Remote Sensing to Forest Ecology and Management." *One Earth* 2 (5): 405–412. doi: 10.1016/j.oneear.2020.05.001.

Mayamanikandan, T., S. Reddy, R. Fararoda, K.C. Thumaty, M.S.S. Praveen, G. Rajashekar, C.S. Jha, et al. 2022. "Quantifying the Influence of Plot-Level Uncertainty in Above Ground Biomass up Scaling Using Remote Sensing Data in Central Indian Dry Deciduous Forest." *Geocarto International* 37 (12): 3489–3503. doi: 10.1080/10106049.2020.1864029.

Næsset, E., T. Gobakken, J. Holmgren, H. Hyyppä, J. Hyyppä, M. Maltamo, M. Nilsson, et al. 2004. "Laser Scanning of Forest Resources: The Nordic Experience." *Scandinavian Journal of Forest Research* 19 (6): 482–499. doi: 10.1080/02827580410019553.

Naesset, E. 2001. "Effects of Differential Single-and Dual-Frequency GPS and GLONASS Observations on Point Accuracy under Forest Canopies." *Photogrammetric Engineering and Remote Sensing* 67 (9): 1021–1026.

Nitoslawski, S.A., K. Wong-Stevens, J.W.N. Steenberg, K. Witherspoon, L. Nesbitt, and C.C. Konijnendijk van den Bosch. 2021. "The Digital Forest: Mapping a Decade of Knowledge on Technological Applications for Forest Ecosystems." *Earth's Future* 9 (8): e2021EF002123. doi:10.1029/2021EF002123.

Oh, S., J. Jung, G. Shao, G. Shao, J. Gallion, and S. Fei. 2022. "High-Resolution Canopy Height Model Generation and Validation Using USGS 3DEP LiDAR Data in Indiana, USA." *Remote Sensing* 14 (4): 935. doi: 10.3390/rs14040935.

Pinz, A. 1991. "A Computer Vision System for the Recognition of Trees in Aerial Photographs." *Multisource Data Integration in Remote Sensing* 3099: 111–124.

Pirsiavash, Ali, Ali Broumandan, Gérard Lachapelle, and Kyle O'Keefe. 2019. "Detection and De-Weighting of Multipath-Affected Measurements in a GPS/Galileo Combined Solution." In 2019 European Navigation Conference (ENC), 1–11. Warsaw, Poland: IEEE.

Tang, H., J. Armston, S. Hancock, S. Marselis, S. Goetz, and R. Dubayah. 2019. "Characterizing Global Forest Canopy Cover Distribution Using Spaceborne Lidar." *Remote Sensing of Environment* 231 (September): 111262. doi: 10.1016/j.rse.2019.111262.

Tomaštík, J., M. Mokroš, S. Saloň, F. Chudý, and D. Tunák. 2017. "Accuracy of Photogrammetric UAV-Based Point Clouds under Conditions of Partially-Open Forest Canopy." *Forests* 8 (5): 151. doi: 10.3390/f8050151.

Trimble. 2020. "Advanced Multipath Mitigation." Technologies. December 2020. https://oemgnss.trimble.com/technologies/advanced-multipath-mitigation/.

USDA Forest Service. 2016. "Field Data Collection Procedures for Phase 2 Plots." In *Forest Inventory and Analysis National Core Field Guide*, 7th ed. Vol. 1.

White, J.C., N.C. Coops, M.A. Wulder, M. Vastaranta, T. Hilker, and P. Tompalski. 2016. "Remote Sensing Technologies for Enhancing Forest Inventories: A Review." *Canadian Journal of Remote Sensing* 42 (5): 619–641. doi: 10.1080/07038992.2016.1207484.

Wing, M., and J. Frank. 2011. "An Examination of Five Identical Mapping-Grade Global Positioning System Receivers in Two Forest Settings." *Western Journal of Applied Forestry* 26 (3): 119–125.

Wing, M.G. 2008. "Consumer-Grade Global Positioning Systems (GPS) Receiver Performance." *Journal of Forestry* 106 (4): 185–190. doi: 10.1093/jof/106.4.185.

Wulder, M., K.O. Niemann, D.G. Goodenough. 2000. "Local Maximum Filtering for the Extraction of Tree Locations and Basal Area from High Spatial Resolution Imagery." *Remote Sensing of Environment* 73 (1): 103–114. doi:10.1016/S0034-4257(00)00101-2.

Zhang, D., J. Liu, W. Ni, G. Sun, Z. Zhang, Q. Liu, and Q. Wang. 2019. "Estimation of Forest Leaf Area Index Using Height and Canopy Cover Information Extracted From Unmanned Aerial Vehicle Stereo Imagery." *IEEE Journal of Selected Topics in Applied Earth Observations and Remote Sensing* 12 (2): 471–481. doi: 10.1109/JSTARS.2019.2891519.

Zhang, D. 2019. "Costs of Delayed Reforestation and Failure to Reforest." *New Forests* 50 (1): 57–70. doi: 10.1007/s11056-018-9676-y.

Zhao, K., S. Popescu, and R. Nelson. 2009. "Lidar Remote Sensing of Forest Biomass: A Scale-Invariant Estimation Approach Using Airborne Lasers." *Remote Sensing of Environment* 113 (1): 182–196. doi: 10.1016/j.rse.2008.09.009.